ADVANCED ENERGY MATERIALS
www.advenergymat.de

Computational Investigation of MAX as Intercalation Host for Rechargeable Aluminum-Ion Battery

Lin Wang, Jingyang Wang, and Bin Ouyang**

Layered carbides and their analogs with MAX phase (general formula $AM_{n+1}X_n$) have emerged as promising candidates for energy storage and conversion applications. One frontier for energy storage is using MAX as an Al-ion intercalation electrode. Given that many MAXs have Al as the A sites, the structure can potentially serve as a stable host for Al intercalation. Here in this work, 425 ternary MAX Al-ion battery electrodes are computationally enumerated. Specifically, first principal phase diagram calculations are performed on the combinatorial space of 17 types of typical transition metals, five types of anions (C, N, B, Si, and P), three types of stoichiometries (n = 1, 2, and 3) and two types of layered stackings (α and β). Among all the ternary MAX materials, 44 candidates show reasonable synthetic accessibility, and six with extraordinary performance are predicted to be promising Al-ion battery electrodes. With the phase stability, and electrochemical performance (average voltage, theoretical capacity, energy density, and Al diffusion barrier), the work provides a comprehensive computational assessment of the great opportunities behind MAX-based Al-ion batteries.

1. Introduction

MAX phases are a family of layered transition metal carbides/nitrides with the general chemical formula $M_{n+1}AX_n$ (n = 1, 2, and 3), where M represents a transition metal, A represents a group 13–16 elements, and X represents carbon or nitrogen. Along the *c*-axis, layers of $M_{n+1}X_n$ constructed by edge-sharing M_6X octahedra are interleaved by layers of A element, forming an alternative crystal stacking. The in-plane M—X bonds are relatively strong, compared to the intra-plane M—A bonds, both of which constitute a mixed covalent-ionic-metallic bonding nature.[1] Therefore, MAX phases exhibit a unique combination of metallic and ceramic properties: they are electrically and thermally conductive, machinable, and ductile like metals, in the meantime having good oxidation and corrosion resistance, and high-temperature strength like ceramics,[2–4] making them attractive candidates for electrical contacts, thermal shock resistant refractory materials, protective coatings, structural materials for high-temperature applications. MAX phases form in a hexagonal crystal lattice with space group $P6_3/mmc$. (**Figure 1**) When n equals 1, they crystallize in the simplest form, M_2AX (211), in which M, A, and X sit in the *4f*, *2d*, and *2a* Wyckoff sites, respectively. The 211 MAX phase is isostructural with the P2-type alkali layered oxides. When n becomes >1, the number of the 2D $[M_2X]$[5] sheets separating the A layers increases, composing a thicker $M_{n+1}X_n$ layer, while the A layer remains identical. Moreover, for n equals 2 (312) and 3 (413), the relative position of A and $M_{n+1}X_n$ layers may vary, and create two different MAX polymorphs, denoted as α and β. As shown in Figure 1, for both the 312 and 413 phases, the α and β polymorph have an identical $M_{n+1}X_n$ skeleton, however, in the α polymorph the A elements sit in the prismatic sites edge-sharing with the adjacent M_6X octahedra, while in the β polymorph, the prismatic sites of A and the adjacent M_6X octahedra are face-shared. It is worth noting that as the number of n increases, stacking faults[6] may occur in the *a*-*b* plane of the $M_{n+1}X_n$ block and create polymorphs with different stacking sequences.[7]

Given the fact that M—A bonds are chemically more active than M—X bonds, MAX phases can be transformed into their 2D counterparts, MXene, by selectively etching the A element. The first MXene phase $Ti_3C_2T_x$ (T refers to surface terminations such as F, OH, etc. adsorbed in the etching solution) was successfully synthesized from Ti_3AlC_2 in 2011,[8] since when the MXene family has attracted significant attention because of their promising performance for energy storage applications such as batteries, capacitors, electro- and photo-catalysis.[9,10] Metal ions with various sizes including Li,[11,12] Na,[6,13,14] K,[15–17] Mg,[18] and Al[19–21] can be inserted into the layers of MXene, which established a new family of promising electrode materials, especially for multivalent ions (Mg^{2+}, Al^{3+}) for which suitable intercalation host materials are currently scarce. Among all potential cathode materials

L. Wang, B. Ouyang
Department of Chemistry and Biochemistry
Florida State University
Tallahassee, FL 32304, USA
E-mail: lw22@fsu.edu; bo22b@fsu.edu
J. Wang
Department of Materials Science and Engineering
University of California
Berkeley, CA 94720, USA
E-mail: jingyang_wang@berkeley.edu
J. Wang
School of Sustainable Energy and Resources
School of Materials Science and Intelligent Engineering
Nanjing University
Suzhou 215163, P. R. China

The ORCID identification number(s) for the author(s) of this article can be found under https://doi.org/10.1002/aenm.202302584

DOI: 10.1002/aenm.202302584

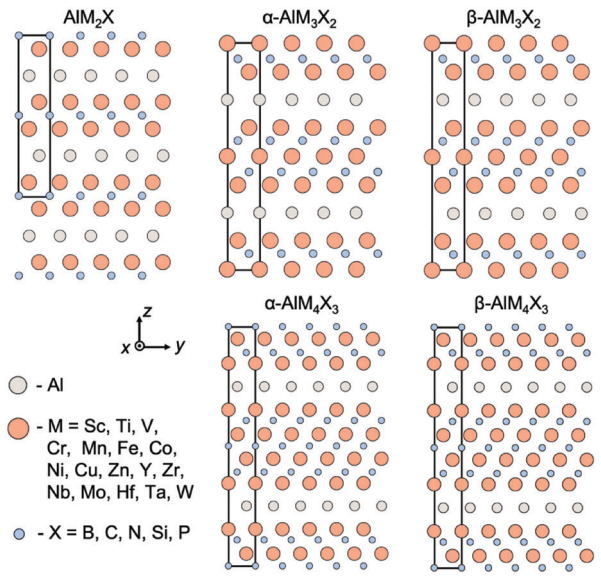

Figure 1. Crystal structures of various MAX phases, i.e., AlM_2X, AlM_3X_2, AlM_4X_3. For AlM_3X_2 and AlM_4X_3, there exist two different phases, α and β, which only differ in the way of Al stackings. For the α phase, Al ions are aligned to the second adjacent M layer, while for the β phase, Al ions are aligned with to first adjacent X layer.

for Al-ion batteries, MAX stands out due to their extraordinary electronic conductivity, the capability of containing only earth-abundant composition, as well as the layered bond topology.[22–24] Additionally, MAX can be made into different nanostructures, such as MXene nanosheets, which allows additional space for tuning the electrochemical performance.[21] In a recent study, layered V_2CT_x was investigated as a cathode material for Al-ion batteries, showing its unique performance for intercalating high-charge-density Al^{3+} ions.[21] It was found out that from multi-layered V_2CT_x to few-layered 2D V_2CT_x sheets, as the number of layers decreased, the electrochemical performance improved significantly.[21]

To date, more than 155 MAX and 20 MXene phases have been discovered.[7,25] The structural (e.g., number of layers, in-plane and out-of-plane transition metal ordering) and chemical (e.g., M, X element, terminal group) versatility greatly enrich the number of compounds in the MAX/MXene family which enable tunable electrochemical properties as electrode materials. Herein, we comprehensively investigate the chemical diversity of the MAX phases with A = Al via high-throughput first-principles calculation. By computationally mapping the chemical formula $M_{n+1}AlX_n$ with n = 1, 2, 3, and various M, X species, the phase stability of 425 MAX compounds was first evaluated via high-throughput density functional theory (DFT) calculations. Among the predicted stable/metastable MAX compounds, the electrochemical properties such as capacity, intercalation voltage, and Al diffusion barrier were theoretically examined as cathode materials for Al-ion batteries.

2. Methodology

The DFT calculations were performed using the Vienna ab initio simulation package (VASP)[26] and projector-augmented wave (PAW) method.[27] For each of the structural optimization calculations, a reciprocal space discretization of 25 Å was applied, and the convergence criteria were set to 10^{-6} eV for electronic loops and 0.02 eV A^{-1} for ionic loops. To address more accurate energetics in the layered structure, the state-of-the-art meta-GGA method r^{2}SCAN[28] was used for structural relaxation and has been benchmarked to be superior for predicting stability[28–30] and geometry. The Van der Waals interaction is considered with rVV10 functional.[31] For all DFT calculations, a supercell of $4 \times 4 \times 1$ is constructed to avoid unphysical interactions between periodic images. To calculate activation barriers for Al diffusion, climb-image Nudged Elastic Band method (ci-NEB)[32] has been applied with DFT relaxed structures.

The theoretical capacity demonstrated is determined by the material mass and electron transfer number, calculated by the equation below, where F is the Faraday constant, M represents Molar mass (g mol^{-1}) of the $M_{n+1}X_n$ component and n represents the charge state of the carrier:

$$C_{\text{Theory}} = \frac{F \times n}{3.6 \times M} \tag{1}$$

The average voltages are calculated as:

$$V_{\text{Avg}} = \frac{E\left(AlM_{n+1}X_n\right) - E\left(M_{n+1}X_n\right) - \mu\left(Al\right)}{3e^-} \tag{2}$$

3. Results

3.1. High-Throughput Calculations and Phase Stability Investigation for MAX

High throughput phase diagram calculations were conducted to evaluate the phase stability of the MAX phases with the chemical formula $M_{n+1}AlX_n$ (n = 1, 2, and 3). As summarized in **Figure 2**,

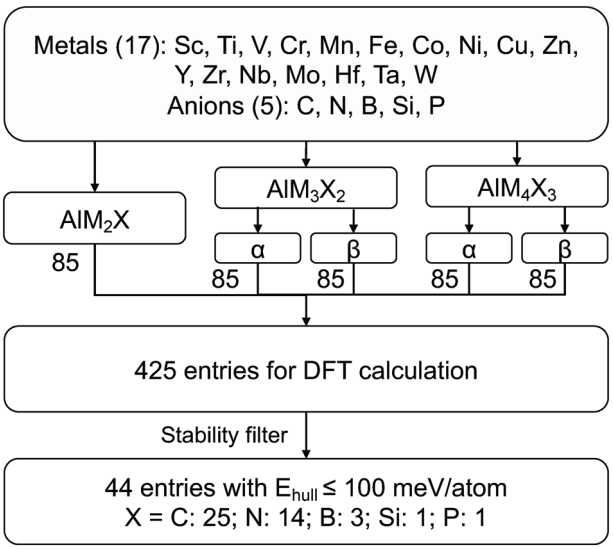

Figure 2. High-throughput calculations workflow. In total 425 MAX entries were evaluated. 44 entries were found with energy above the hull (E_{hull}) ≤100 meV $atom^{-1}$.

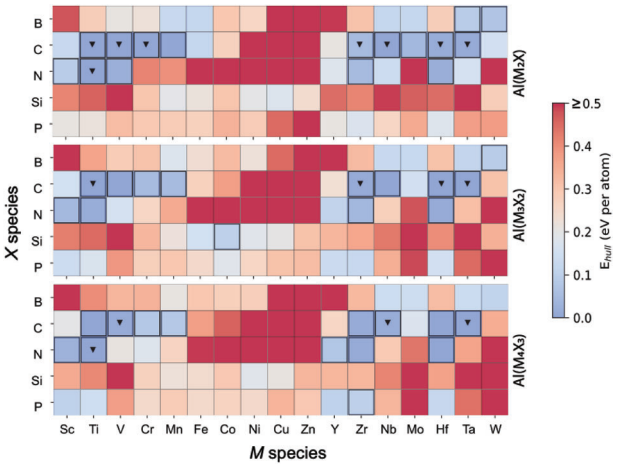

Figure 3. Color-coded stability map of calculated MAX compounds. Stable and metastable compounds with E_{hull} <100 meV atom^{-1} are highlighted by squares, while triangles denote experimentally reported ones. For each composition in the AlM_3X_2 and AlM_4X_3 categories, the lowest energy stacking (α or β) is selected to construct the map.

for each value of n, 17 metal (M) and 5 anion (X) species were considered, leading to 85 different compositions per prototype composition. For structures with $n = 2$, 3, two types of layered stackings (α and β) were included, differing only in the relative position of Al ions: Al-ions in α-phase are placed on top of the second adjacent metal site, while Al-ions in β-phase are placed on top of the nearest anion site. These high-throughput settings resulted in 425 MAX compounds in total for DFT calculations.

The synthetic accessibility of each compound was evaluated by constructing the compositional phase diagram that includes all phases in the specifical M—A—X compositional spaces obtained from Materials Project.[33] The energy above hull (E_{hull}) is used for assessing the phase stability.[34] By setting an E_{hull} ≤100 meV atom^{-1} as the boundary for selecting synthetic accessible compounds, which is a reasonable estimation for materials' metastability,[35] 44 entries were obtained as thermodynamically stable or metastable phases (Figure 2).

The phase stability of MAX compounds as a function of M, X species is demonstrated by the color-coded E_{hull} map shown in **Figure 3**. For the compositions AlM_3X_2 and AlM_4X_3, the lower E_{hull} value between α and β stacking is presented. In Figure 3, all experimental synthesized Al-containing MAX phases,[7,25] as denoted by the triangles, are correctly classified as stable/metastable (E_{hull} ≤100 meV atom^{-1}), indicating the capability of our calculation results for predicting new materials. Besides the experimental reported ones, another 28 new MAX materials were found to be promising synthesizable materials.

The synthetic accessibility of MAX phases exhibits distinct trends concerning anion and metal chemistry. Regarding anion species, the majority of stable/metastable MAX identified are either carbides or nitrides, aligning with their prevalent in existing literatures. B, Si, and P are found to be somewhat compatible with only a few second-, third-row transition metals, i.e., $AlTa_2B$, AlW_2B, AlW_3B_2, and $AlZr_4P_3$, while the only metastable MAX containing the first-row transition metal with B, Si or P as anion is $AlCo_3Si_2$. In terms of metal species, early transition metals tend to be more stable in a MAX structure than late transition metals. For instance, Ti, V, Cr, and Mn all have stable/metastable carbides, whereas Fe, Co, Ni, Cu, and Zn do not. Similarly, Zr, Nb, Hf, and Ta can also form stable/metastable carbide structure. Nitrides favor early transition metals as well but are generally less stable than carbides. These trends collectively indicate that the redox metals commonly utilized in current Li-, Na-ion cathodes are not compatible with the Al-MAX structure, at least based on our E_{hull} criterion.

To investigate the ground-state stacking of the calculated AlM_3X_2 and AlM_4X_3 compounds, the relative stability of the α and β stacking (quantified by $E_{hull,\alpha} - E_{hull,\beta}$) is calculated and plotted in **Figure 4**. Compositions with $E_{hull,\alpha} - E_{hull,\beta}$ <0 indicate a preference for α stacking, while those with $E_{hull,\alpha} - E_{hull,\beta}$ >0 favors β stacking. The majority of compositions show α stacking as the ground state, with only 21 and 22 compositions favoring β stacking in the AlM_3X_2 and AlM_4X_3 family, respectively. Although the E_{hull} difference between those two stackings is generally small, for certain compositions such as AlW_3Si_2, $AlZn_3C_2$, $AlZn_4C_3$, $AlZn_4N_3$, etc., it can be as large as 300 meV atom^{-1}. Since the α and β stacking only differ in the position of Al ions relative to the $M_{n+1}X_n$ skeleton, it reveals that a large E_{hull} difference translates to a large energy difference for different Al sites, thereby a large migration barrier for Al hopping will be expected. In addition, it is worth noting that the 44 stable/metastable compounds are all α stacking favorable, therefore, electrochemical performance as Al-ion battery is only evaluated for the stable/metastable α phases in the later section.

3.2. Average Voltage, Capacity, and Energy Density as Al-Ion Battery Electrode

Electrochemical performance is then evaluated for the 44 computationally screened stable/metastable compounds. In addition to E_{hull} value, the average voltage, theoretical capacity, and corresponding energy density as computed as shown in **Table 1**. It has been seen that MAX materials typically exhibit high capacity and energy density. The majority of MAX materials exhibit a notable high capacity with 24 of them (bold in Table 1) having a capacity >274 mAh g^{-1}, which is the capacity of $LiCoO_2$.

In addition to Table 1, the calculated voltage (with a range from 0.203 to 1.039 V) of 44 metastable/stable MAX materials is also plotted in **Figure 5**a for better comparison. We found that the voltage is largely determined by the metal and anion species rather than the stacking sequences, moreover, nitrides exhibit higher voltages compared to carbides in common, which can be attributed to the similarity in terms of bond covalency between nitrides and carbides. This is different from the case of Na/K and multivalent contained metal oxides, where Alkali (earth) metal interactions significantly influence the voltage. [36,37]

Figure 5b presents the energy density (with a range from 40.99 to 386.87 Wh kg^{-1}) of 44 metastable/stable MAX materials. 18 out of 44 have an energy density higher than 165 Wh kg^{-1}, which is the capacity offered by commercialized $LiCoO_2$.[38] It is also very straightforward to see that AlM_2X shows the highest theoretical capacity compared with other stacking, solely due to the higher mole fraction of Al per formula unit.

Table 1. Calculated MAX compounds with energy above the hull <100 meV atom^{-1}. Asterisk (*) denotes experimentally reported ones.[7]

#	Type	Formula	E_{hull} [meV atom^{-1}]	Voltage [V vs Al]	Capacity [mAh g^{-1}]	Energy density [Wh kg^{-1}]
1	AlM_2X	$AlSc_2N$	91.19	0.288	773.72	222.87
2		$AlTi_2C$*	0.11	0.434	746.25	323.99
3		$AlTi_2N$*	−0.003	0.490	732.67	359.29
4		AlV_2C*	−0.03	0.548	705.96	386.87
5		AlV_2N	19.46	0.488	693.80	338.89
6		$AlCr_2C$*	−11.46	0.467	693.12	323.66
7		$AlMn_2C$	−20.59	0.463	659.66	305.67
8		$AlZr_2C$*	45.08	0.376	413.48	155.52
9		$AlZr_2N$	47.98	0.498	409.28	203.89
10		$AlNb_2C$*	0.014	0.604	406.44	245.74
11		$AlMo_2C$	40.13	0.530	394.35	209.16
12		$AlHf_2C$*	13.38	0.427	217.90	92.94
13		$AlHf_2N$	16.31	0.548	216.73	118.84
14		$AlTa_2B$	89.52	0.641	215.73	138.21
15		$AlTa_2C$*	7.953	0.644	215.04	138.38
16		AlW_2B	70.99	0.631	212.43	134.01
		16 (8 new) compounds have E_{hull} <100 meV atom^{-1}				
1	AlM_3X_2	$AlSc_3N_2$	41.95	0.282	493.64	139.12
2		$AlTi_3N_2$	12.70	0.496	479.67	203.23
3		$AlTi_3C_2$*	−0.03	0.424	468.52	232.50
4		AlV_3C_2	1.81	0.524	454.66	238.21
5		$AlCr_3C_2$	48.51	0.406	446.67	181.20
6		$AlMn_3C_2$	46.12	0.423	425.79	180.14
7		$AlCo_3Si_2$	97.86	1.039	345.13	358.68
8		$AlZr_3C_2$*	10.04	0.371	270.09	100.10
9		$AlZr_3N_2$	37.41	0.520	266.52	138.62
10		$AlNb_3C_2$	−0.04	0.587	265.59	155.92
11		$AlHf_3C_2$*	−16.97	0.413	143.71	59.46
12		$AlHf_3N_2$	10.82	0.572	142.69	81.55
13		$AlTa_3C_2$*	−0.02	0.645	141.84	91.54
14		AlW_3B_2	92.81	0.564	140.29	79.18
		14 (10 new) compounds have E_{hull} <100 meV atom^{-1}				
1	AlM_4X_3	$AlSc_4N_3$	26.71	0.282	362.44	102.23
2		$AlTi_4N_3$*	0.06	0.517	353.42	151.77
3		$AlTi_4C_3$	−3.63	0.429	344.36	177.93
4		AlV_4C_3*	9.08	0.551	335.30	184.66
5		$AlCr_4C_3$	77.31	0.371	329.50	122.19
6		$AlMn_4C_3$	81.17	0.389	314.34	122.13
7		AlY_4N_3	74.56	0.203	202.20	40.99
8		$AlZr_4C_3$	10.02	0.378	200.55	75.90
9		$AlZr_4N_3$	11.56	0.511	197.59	101.05
10		$AlZr_4P_3$	97.92	0.500	197.23	112.30
11		$AlNb_4C_3$*	12.36	0.569	175.63	87.74
12		$AlHf_4C_3$	−15.67	0.426	107.21	45.62
13		$AlHf_4N_3$	−8.77	0.569	106.36	60.53
14		$AlTa_4C_3$*	−0.05	0.602	105.82	63.67
		14 (10 new) compounds have E_{hull} <100 meV atom^{-1}				

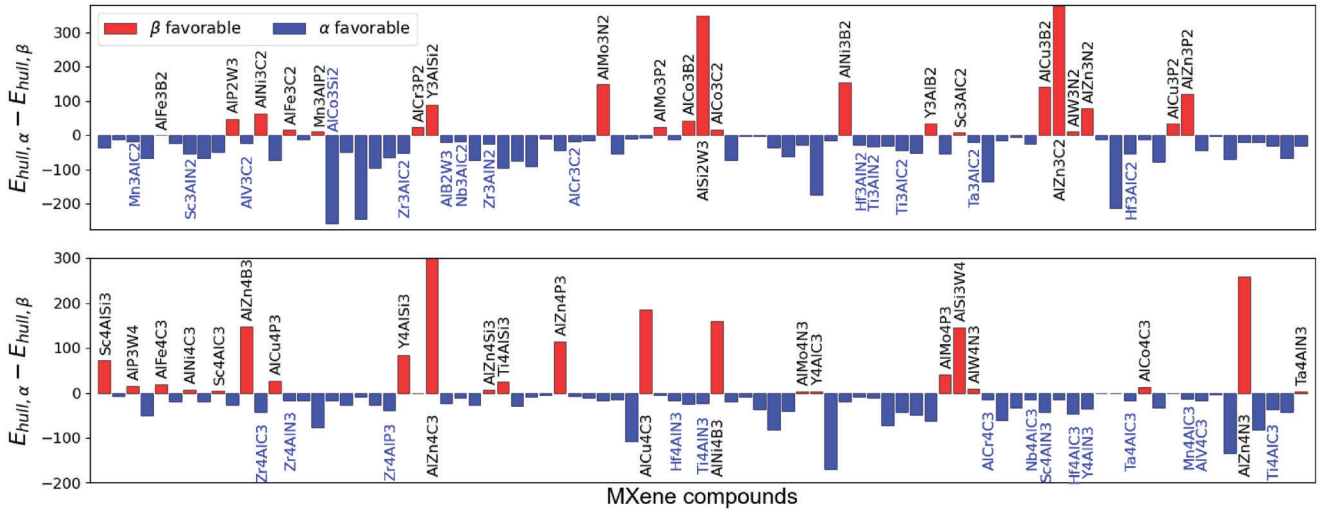

Figure 4. Calculated E_{hull} difference between α phase and β phase for AlM_3X_2 (top) and AlM_4X_3 (bottom). β-favorable compounds have positive $\triangle E_{hull}$ values, which are represented by red histograms and annotated. α-favorable compounds are represented by blue histograms. Stable and metastable phases ($E_{hull} \leq 100$ meV atom^{-1}) are also annotated in blue. Note that all stable and metastable phases are α-favorable.

It is interesting to see that the only silicide that is predicted to be synthetic accessible, $AlCo_3Si_2$, demonstrates impressively high voltage (1.039 V) and energy density (321.44 Wh kg^{-1}), but the large activation energy makes Al hard to diffuse. To ensure intrinsic stability and limited influence of stability from the fluctuation of Al intercalation, E_{hull} in both aluminated state and dealuminated state are taken into consideration (listed in Table S1, Supporting Information). Combining the electrochemical properties, six promising candidates are proposed to be good candidates, e.g. $AlSc_3N_2$, $AlTi_2C$, $AlZr_4C_3$, $AlZr_3C_2$, $AlZr_4N_3$, and $AlTi_4C_3$, some of which have already been reported in experiments.[39] Since these materials show reasonable E_{hull} values in both aluminated and dealuminated states, they will be reasonably stable at different Al-ion concentrations. It cannot be denied that when most Al-ions are completely removed from the host material, there could be layers of cavities in these materials, which may lead to collapse of structure.[40] Such an issue has already been well addressed in Li-ion batteries,[29,41,42] in which the Shannon radius of Li^+ (0.76 Å) is even larger than that of Al^{3+} (0.535 Å). Therefore, the existing of cavity should not be a big concern for Al-ion battery.

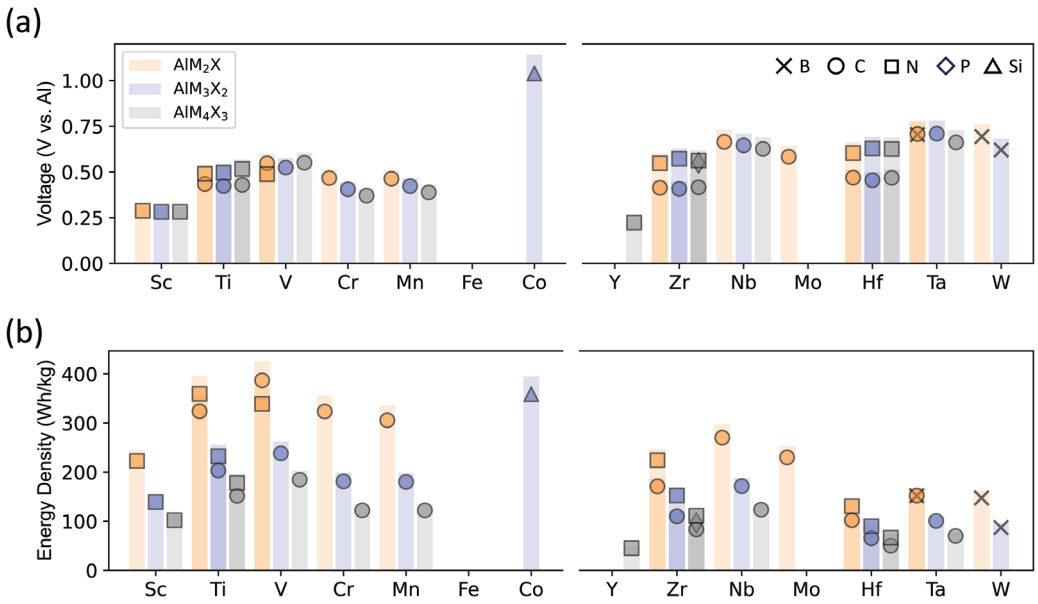

Figure 5. Calculated electrochemical properties for stable/metastable MAX compounds as Al-ion cathodes. MAX polymorphs are represented by different colors: AlM_2X, orange; AlM_3X_2, blue and AlM_4X_3, gray. X species are represented by different symbols: B, cross; C, circle; N, square; Si, triangle and P, diamond. a) theoretical voltage; b) theoretical energy density.

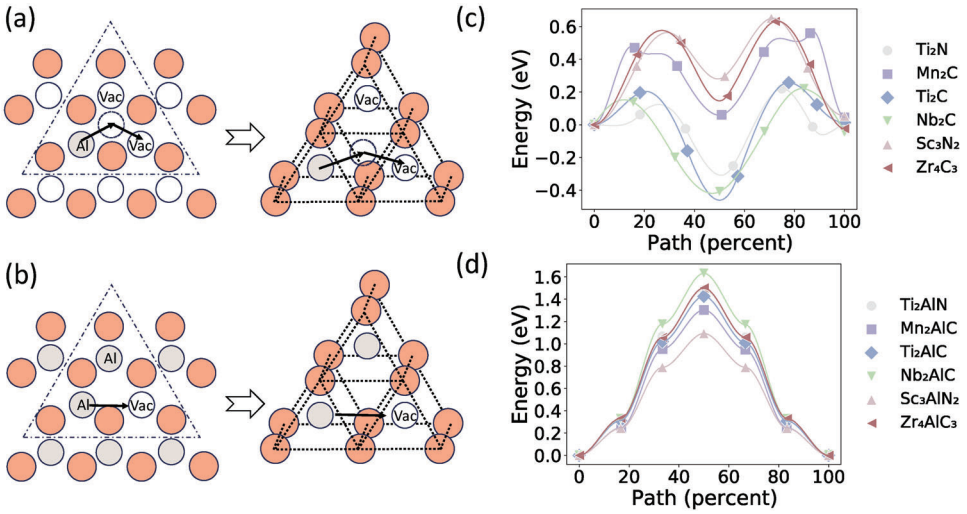

Figure 6. Al migration pathway in MAX through a) dealuminated state; b) aluminated state. The left panels show the top view of diffusion pathway while the right panels show a perspective view. Al, Metal, and vacancy are shown as grey, orange, and white spheres. Energy along the migration pathway in different Al-vacancy environments: c) dealuminated state; d) aluminated state.

3.3. Al Diffusion Barriers

In addition to the thermodynamic properties, the kinetic behavior is also evaluated with ci-NEB calculations (detailed in Methodology). The diffusion of naked Al-ion is considered in the calculations. Two critical concentrations of Al-ions are examined:, i.e., the state when there is dilute concentration of Al vacancy (aluminated state), and the state when there is a dilute concentration of Al-ion (dealuminated state). To model these two states, we remove one Al (for aluminated state) or keep only one Al (for dealuminated state) respectively based on the DFT relaxed fully aluminated structure. We computed the diffusion barrier for both aluminated and dealuminated states for all 44 systems that are stable/metastable. Six materials with lowest Al hopping barriers in the dealuminated state and reasonable barriers in aluminated state are presented in **Figure 6**. The projection from the top view of the layered structure has been presented in Figure 6a,b. Al ions are shown with grey circles and the metals are shown in orange circles. To show the arrangement of the atoms more clearly, a perspective view of the diffusion pathways was drawn in the right panel of Figure 6a,b.

It has been found that the diffusion pathways differ between the aluminated states and dealuminated states, which can be illustrated by the arrows in Figure 6a,b and supported by the minimum energy pathway shown in Figure 6c,d. More specifically, Figure 6a illustrates that the Al hopping at dealuminated state is through a zigzag pathway that goes through the unoccupied prismatic site, which is occupied in the polymorph of β-phase. As a result, the saddle point will be the center of an empty square formed by four metals between two prismatic sites and there will be two saddle points for such ion hoping (shown in Figure 6c). The unoccupied prismatic site will serve as a local minimum during the diffusion pathway. On the other hand, for the aluminated states, Al-ions will diffuse through a straight line between the Al-ion and the adjacent vacancy site, as depicted in Figure 6d. Consequently, there will be no local minimum along the diffusion pathway. The concentration-dependent diffusion mechanism is akin to that observed in Li diffusion within layered metal oxide.[5,43] In both cases, when most of the adjacent Al sites (in the case of MAX phases) or Li sites (in the case of layered metal oxides/chalcogenides) will activate metastable intermediates states through the diffusion pathway.

Additionally, it has been found that in general, the diffusion barrier is much lower in dealuminated states compared with aluminated states, this also forms an interesting consistency with the case of Li diffusion mechanism[43] in layered oxide, where Li diffusion is primarily driven by local clustering of vacancies (e.g., tri-vacancy mechanism[43]). With the observations in **Figure 7**, we conclude that Al diffusion will also be facilitated by the local clustering of vacancy during electrochemical cycling.

With the understanding of vacancy-assisted Al diffusion, we can then estimate the boundary of Al diffusion using the aluminated and dealuminated states (shown in Figure 7). To be more specific, such two states will dictate the upper bound and lower bound of the Al-ion diffusion barrier. Therefore, the range of the colored bar shown in Figure 7 will provide a useful estimation of the range of diffusion barriers at different Al-ion concentrations. All the compositions are ascendingly sorted by the barrier energy of the aluminated state. As inferred from Figure 7, it is generally true that the aluminated state shows a higher activation energy than dealuminated state. However, there are also 6 exceptions ($AlTa_2B$, $AlTa_2C$, $AlZr_4N_3$, AlW_2B, $AlZr_4P_3$, and $AlHf_3N_2$) out of the 44 systems. Moreover, we have found that 18 MAX exhibits barrier energy of <2 eV atom^{-1} under both aluminated and dealuminated states, which can be considered as a battery electrode with a practical diffusion barrier, the dashed line is drawn in Figure 7 to separate these candidates with the other materials that show high diffusion barrier. Note that our calculation results here only represent the maximum value of the Al migration barrier in the bulk phase, as MAX phases can be delaminated to form their 2D counterpart, MXene, in which the migration barrier may be lower. Moreover, the diffusion of Al-ion at cathode/electrolyte interface and liquid electrolyte will involve very different considerations, which are not involved in the current work. Additionally,

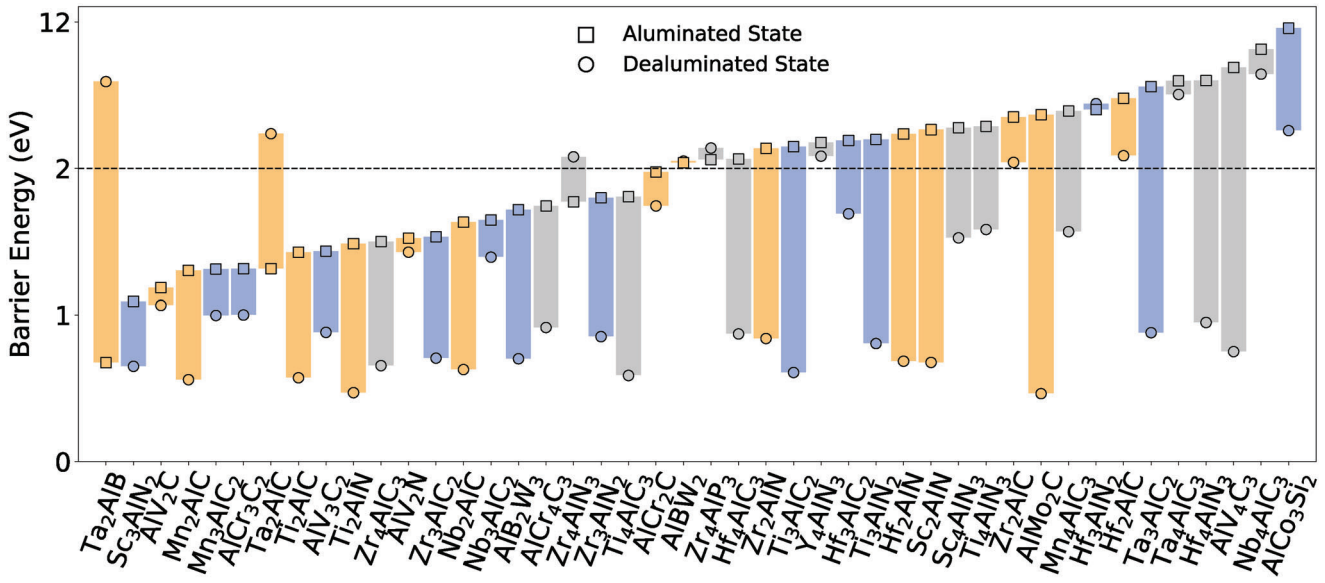

Figure 7. A vertical bar chart showing the activation barrier energy for a single vacancy diffusion (aluminated State) and a single Al diffusion (dealuminated state) for the calculated stable/metastable MAX phases: AlM_2X, orange; AlM_3X_2, blue and AlM_4X_3, gray. Square represents the energy for aluminated state and circle shows that of dealuminated state. The y scale above 2 eV is reduced to show better the barriers within 0–2 eV.

electronic structures are considered in evaluating performance. The density of state (DOS) of all 44 materials shows a neglectable band gap (Figures S1–S7, Supporting Information). Such observations agree with the general claim that MAX shows great electronic conductivity, which also indicates electronic conductivity should not be an issue if MAX is used as electrodes, unlike some cases in transition metal oxide-based electrodes.[4,44]

4. Discussion

When calculating the migration pathway and barrier, only naked aluminum (Al) ions without the involvement of electrolyte because our primary focus was on the intrinsic bulk properties of MAX phases in the context of Al-ion batteries. Such analyses have been widely used to help rapidly identify promising multivalent electrodes as well as further guide experimental design.[37,45] At the same time, comparable barriers (<1 eV) in some candidates are in line with state-of-the-art Li-ion and Na-ion batteries,[46,47] which also indicates that it is feasible to achieve reasonable Al-ion diffusion barriers with careful compositional design.

Given that the MAX phase shows stability across diverse combinations of metals and anions, the synthetic chemical space is broad for making an Al-ion battery out of MAX phases. To assess the practicality of using MAX phases as Al-ion cathodes in comparison with other Al-ion battery cathodes, the electrochemical performance of reported Al-ion electrodes is summarized in **Figure 8**, which can be classified as organic, carbon-based, and compound electrodes. We want to clarify that Figure 8 is a combination of computational data and experimental data with different testing conditions, which can facilitate the understanding of the potential of MAX as Al-ion battery compared with other existing materials. However, the predicted electrochemical performance for MAXs should not be over-considered as a guaranteed performance for MAX-based Al-ion battery.

In general, the MAX phases predicted in this study exhibit superior theoretical capacity, particularly when compared with carbon-based electrodes and organic electrodes. However, the average voltage of MAX phases is generally lower than carbon-based and organic electrodes, resulting in similar energy density for many MAX phases and carbon/organic electrodes. Nevertheless, it is important to note that certain candidates, such as V_2C, Ti_2C, Ti_2N, V_2N, and Mn_2C, exhibit higher energy density than most of the organic and carbon-based electrodes. There are some V-based and Ti-based compounds being confirmed as promising battery materials.[39,80,81] This suggests that MAX phases have the potential to deliver competitive energy density in practical applications. Furthermore, the distribution of compound electrodes appears similar to that of MAX phases. This is largely because these compounds are mostly with different crystal structures but similar layered like bond topology, such as $MoSe_2$[48] and $CoSe_2$.[61] The intercalation mechanism is similar for these materials with respect to MAX.

Finally, we also want to make several other remarks on the design of the MAX-based battery. Most of the MAX will be stabilized with C and N as anion and refractory metal as cation. This can be originated from redox compatibility, as late transition metals (such as Ni and Co) typically show much higher oxidizing potential compared with B/C/N/Si/P. This can be represented by the case of Ni_4C_3, while the incompatibility between high oxidizing Ni^{3+} and highly reductive C^{4-} will bring in the strong competing phase of Ni and C as an elemental phase. All the competing phases are listed in Table S2 (Supporting Information), while in general, the late transition metals will tend to have competing phases that possess oxidized anion and reduced cation. Moreover, it is interesting to see that we can extend Al-based MAX into much broader chemistry, as multiple silicides, phosphides, and borides-based MAX are identified to be stable based on our phase diagram calculations,

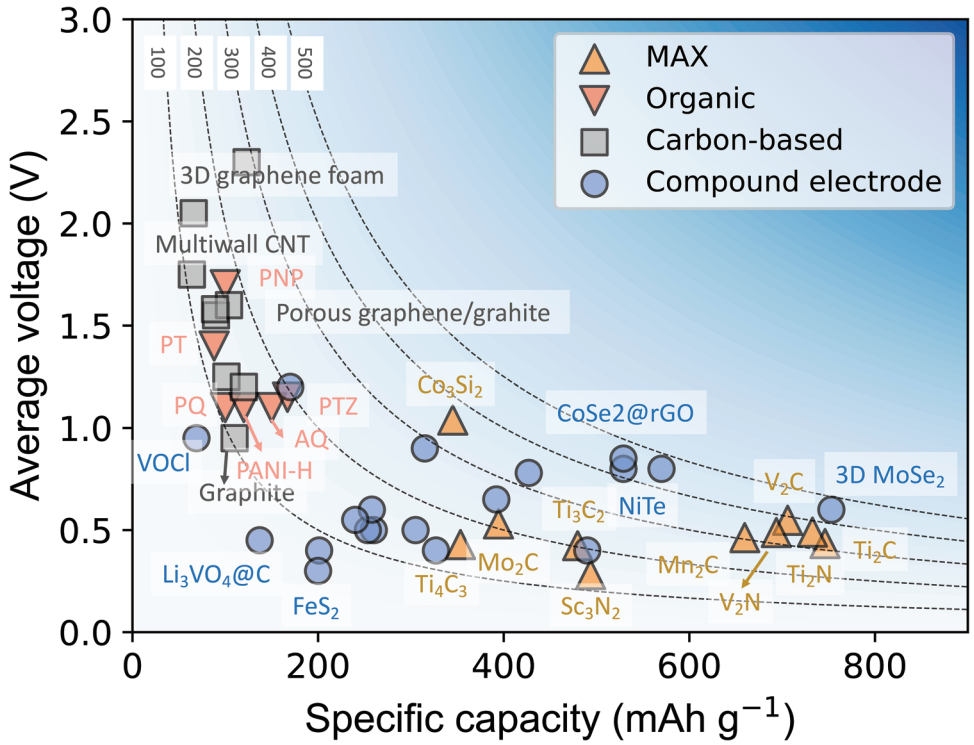

Figure 8. Comparison of energy density and average voltage with other reported Al-ion batteries.[48–79] All the data are classified into four groups, MAX (yellow up triangle), Organic (tomato down triangle), Carbon-based (grey square), and Compound electrode (blue circle) Al-ion batteries. The gradient of blue represents the energy density gradient, with curves showing 100, 200, 300, 400, and 500 Wh kg^{-1}.

which will allow for more tunable space for electrochemical performance.

It is also worth noting that MAX in general has low redox potential, mainly due to the low oxidization potential of refractory metals and MAX-favored anions (e.g., C, N, B, Si, and P). However, this can be improved by the functionalization and designing of various heterostructures. In the emerging field of MXene, O, OH, and F groups are widely applied as functionalization groups,[48,82,83] which also leads to significant improvement of voltage as reported in several recent works. [21,80,20,84] This is mainly because a) the surface functionalization elevates the average charge states of metal, primarily through the incorporation of negatively charged ions. This effect is particularly pronounced for surface atoms and naturally leads to an increase in the redox voltage. This is especially significant in the context of MXene materials,[21] where surface ion exchange plays a critical role; b) there will also be an inductive effect[85,86] due to the enhanced ionicity between O, F, OH with metal site in MAX phase, which pushes down the electronic state of metal and thus increase its redox potential. Moreover, as shown in Figure 8, the nanostructure of electrodes for carbon has led to a wide range of voltage,[71–79] which also implies that the nanostructured MAX should be able to follow the same path for extending the voltage window.

5. Conclusion

We have presented a complete combinatorial study of 425 single metal-based MAX that can potentially serve as Al-ion battery electrodes. The chemical space consists of 17 different metals, five types of anions, and five types of structures. Systematically evaluations of electrochemical properties have been made in terms of average voltage, theoretical capacity, theoretical energy density, and Al-ion diffusion barrier while five promising new compositions have been proposed as promising candidates for Al-ion battery cathodes. All data presented in the manuscript is also made available via GitHub at https://jeff-oakley.github.io/Al-MAX_data/.

Supporting Information

Supporting Information is available from the Wiley Online Library or from the author.

Acknowledgements

The authors acknowledge support from the startup funding from Florida State University. The Computational resources are provided by the Advanced Cyberinfrastructure Coordination Ecosystem: Services & Support (ACCESS), the National Energy Research Scientific Computing Center (NERSC), a DOE Office of Science User Facility supported by the Office of Science and the U.S. Department of Energy under contract no. DE-AC02-05CH11231 and Research Computing Center (RCC) at Florida State University. The computation and data processing are also supported by the supercomputing resources from the Department of Energy's Office of Energy Efficiency and Renewable Energy at the National Renewable Energy Laboratory.

Conflict of Interest

The authors declare no conflict of interest.

Data Availability Statement

The data that support the findings of this study are available from the corresponding author upon reasonable request.

Keywords

Al-ion batteries, high throughput screening, MAX

Received: August 7, 2023
Revised: October 1, 2023
Published online:

[1] Z. Zhang, X. Duan, D. Jia, Y. Zhou, S. Van Der Zwaag, *J. Eur. Ceram. Soc.* **2021**, *41*, 3851.
[2] Z. M. Sun, *Int. Mater. Rev.* **2013**, *56*, 143.
[3] J. Gonzalez-Julian, *J. Am. Ceram. Soc.* **2020**, *104*, 659.
[4] B. Kang, G. Ceder, *Nature* **2009**, *458*, 190.
[5] A. Van Der Ven, *Electrochem. Solid-State Lett.* **1999**, *3*, 301.
[6] D. Er, J. Li, M. Naguib, Y. Gogotsi, V. B. Shenoy, *ACS Appl. Mater. Interfaces* **2014**, *6*, 11173.
[7] M. Sokol, V. Natu, S. Kota, M. W. Barsoum, *Trends Chem.* **2019**, *1*, 210.
[8] M. Naguib, M. Kurtoglu, V. Presser, J. Lu, J. Niu, M. Heon, L. Hultman, Y. Gogotsi, M. W. Barsoum, *Adv. Mater.* **2011**, *23*, 4248.
[9] B. Anasori, M. R. Lukatskaya, Y. Gogotsi, *Nat. Rev. Mater.* **2017**, *2*, 16098.
[10] M. Gyu Jung, G. Sambhaji Gund, Y. Gogotsi, H. Seok Park, *Batteries Supercaps* **2020**, *3*, 354.
[11] J. Xu, M.-Q. Zhao, Y. Wang, W. Yao, C. Chen, B. Anasori, A. Sarycheva, C. E. Ren, T. Mathis, L. Gomes, L. Zhenghua, Y. Gogotsi, *ACS Energy Lett.* **2016**, *1*, 1094.
[12] S. Zhao, Y. Dall'agnese, X. Chu, X. Zhao, Y. Gogotsi, Y. Gao, *ACS Energy Lett.* **2019**, *4*, 2452.
[13] M.-Q. Zhao, X. Xie, C. E. Ren, T. Makaryan, B. Anasori, G. Wang, Y. Gogotsi, *Adv. Mater.* **2017**, *29*, 1702410.
[14] S.-M. Bak, R. Qiao, W. Yang, S. Lee, X. Yu, B. Anasori, H. Lee, Y. Gogotsi, X.-Q. Yang, *Adv. Energy Mater.* **2017**, *7*, 1700959.
[15] R. Zhao, H. Di, X. Hui, D. Zhao, R. Wang, C. Wang, L. Yin, *Energy Environ. Sci.* **2020**, *13*, 246.
[16] F. Ming, H. Liang, W. Zhang, J. Ming, Y. Lei, A.-H. Emwas, H. N. Alshareef, *Nano Energy* **2019**, *62*, 853.
[17] Y. Wu, Y. Sun, J. Zheng, J. Rong, H. Li, L. Niu, *Chem. Eng. J.* **2021**, *404*, 126565.
[18] M. Xu, S. Lei, J. Qi, Q. Dou, L. Liu, Y. Lu, Q. Huang, S. Shi, X. Yan, *ACS Nano* **2018**, *12*, 3733.
[19] H. Liu, H. Wang, Z. Jing, K. Wu, Y. Cheng, B. Xiao, *J. Phys. Chem. C* **2020**, *124*, 25769.
[20] J. Li, F. Zeng, J. K. El-Demellawi, Q. Lin, S. Xi, J. Wu, J. Tang, X. Zhang, X. Liu, S. Tu, *ACS Appl. Mater. Interfaces* **2022**, *14*, 45254.
[21] A. Vahidmohammadi, A. Hadjikhani, S. Shahbazmohamadi, M. Beidaghi, *ACS Nano* **2017**, *11*, 11135.
[22] L. Zheng, H. Yang, Y. Bai, C. Wu, *Energy Mater. Adv.* **2022**, *2022*, 0005.
[23] L. Zheng, H. Yang, Y. Bai, C. Wu, *J. Energy Chem.* **2021**, *60*, 229.
[24] L. Zheng, Y. Bai, C. Wu, *Chin. Chem. Lett.* **2023**, 108589.
[25] Q. Jiang, Y. Lei, H. Liang, K. Xi, C. Xia, H. N. Alshareef, *Energy Storage Mater.* **2020**, *27*, 78.
[26] G. Kresse, J. Furthmüller, *Comput. Mater. Sci.* **1996**, *6*, 15.
[27] G. Kresse, D. Joubert, *Phys. Rev. B* **1999**, *59*, 1758.
[28] J. W. Furness, A. D. Kaplan, J. Ning, J. P. Perdew, J. Sun, *J. Phys. Chem. Lett.* **2020**, *11*, 8208.
[29] X. Zhao, Y. Tian, Z. Lun, Z. Cai, T. Chen, B. Ouyang, G. Ceder, *Joule* **2022**, *6*, 1654.
[30] Y. Zhang, D. A. Kitchaev, J. Yang, T. Chen, S. T. Dacek, R. A. Sarmiento-Pérez, M. A. L. Marques, H. Peng, G. Ceder, J. P. Perdew, J. Sun, *Npj Comput. Mater.* **2018**, *4*, 9.
[31] H. Peng, Z.-H. Yang, J. P. Perdew, J. Sun, *Phys. Rev. X* **2016**, *6*, 041005.
[32] G. Henkelman, B. P. Uberuaga, H. Jónsson, *J. Chem. Phys.* **2000**, *113*, 9901.
[33] A. Jain, S. P. Ong, G. Hautier, W. Chen, W. D. Richards, S. Dacek, S. Cholia, D. Gunter, D. Skinner, G. Ceder, K. A. Persson, *APL Mater.* **2013**, *1*, 011002.
[34] W. Sun, S. T. Dacek, S. P. Ong, G. Hautier, A. Jain, W. D. Richards, A. C. Gamst, K. A. Persson, G. Ceder, *Sci. Adv.* **2016**, *2*, e1600225.
[35] B. Ouyang, J. Wang, T. He, C. J. Bartel, H. Huo, Y. Wang, V. Lacivita, H. Kim, G. Ceder, *Nat. Commun.* **2021**, *12*, 5752.
[36] Y. Tian, G. Zeng, A. Rutt, T. Shi, H. Kim, J. Wang, J. Koettgen, Y. Sun, B. Ouyang, T. Chen, Z. Lun, Z. Rong, K. Persson, G. Ceder, *Chem. Rev.* **2021**, *121*, 1623.
[37] P. Canepa, G. Sai Gautam, D. C. Hannah, R. Malik, M. Liu, K. G. Gallagher, K. A. Persson, G. Ceder, *Chem. Rev.* **2017**, *117*, 4287.
[38] K. Mizushima, P. C. Jones, P. J. Wiseman, J. B. Goodenough, *Mater. Res. Bull.* **1980**, *15*, 783.
[39] M. Naguib, J. Come, B. Dyatkin, V. Presser, P.-L. Taberna, P. Simon, M. W. Barsoum, Y. Gogotsi, *Electrochem. Commun.* **2012**, *16*, 61.
[40] H. Ding, Y. Li, M. Li, K. Chen, K. Liang, G. Chen, J. Lu, J. Palisaitis, P. O. Å. Persson, P. Eklund, L. Hultman, S. Du, Z. Chai, Y. Gogotsi, Q. Huang, *Science* **2023**, *379*, 1130.
[41] K. G. Naik, B. S. Vishnugopi, J. Datta, D. Datta, P. P. Mukherjee, *Appl. Mech. Rev.* **2023**, *75*, 010802.
[42] J. C. Stallard, L. Wheatcroft, S. G. Booth, R. Boston, S. A. Corr, M. F. L. De Volder, B. J. Inkson, N. A. Fleck, *Joule* **2022**, *6*, 984.
[43] J. Bhattacharya, A. Van Der Ven, *Phys. Rev. B* **2011**, *83*, 144302.
[44] J. Wang, X. Sun, *Energy Environ. Sci.* **2012**, *5*, 5163.
[45] M. Liu, Z. Rong, R. Malik, P. Canepa, A. Jain, G. Ceder, K. A. Persson, *Energy Environ. Sci.* **2015**, *8*, 964.
[46] C. Ouyang, S. Shi, Z. Wang, X. Huang, L. Chen, *Phys. Rev. B* **2004**, *69*, 104303.
[47] S. P. Ong, V. L. Chevrier, G. Hautier, A. Jain, C. Moore, S. Kim, X. Ma, G. Ceder, *Energy Environ. Sci.* **2011**, *4*, 3680.
[48] Y. Ai, S.-C. Wu, K. Wang, T.-Y. Yang, M. Liu, H.-J. Liao, J. Sun, J.-H. Chen, S.-Y. Tang, D. C. Wu, T.-Y. Su, Y.-C. Wang, H.-C. Chen, S. Zhang, W.-W. Liu, Y.-Z. Chen, L. Lee, J.-H. He, Z. M. Wang, Y.-L. Chueh, *ACS Nano* **2020**, *14*, 8539.
[49] T. Cai, L. Zhao, H. Hu, T. Li, X. Li, S. Guo, Y. Li, Q. Xue, W. Xing, Z. Yan, L. Wang, *Energy Environ. Sci.* **2018**, *11*, 2341.
[50] Y. Hu, B. Luo, D. Ye, X. Zhu, M. Lyu, L. Wang, *Adv. Mater.* **2017**, *29*, 1606132.
[51] Y. Hu, D. Ye, B. Luo, H. Hu, X. Zhu, S. Wang, L. Li, S. Peng, L. Wang, *Adv. Mater.* **2018**, *30*, 1703824.
[52] J. Jiang, H. Li, T. Fu, B.-J. Hwang, X. Li, J. Zhao, *ACS Appl. Mater. Interfaces* **2018**, *10*, 17942.
[53] J. Jiang, H. Li, J. Huang, K. Li, J. Zeng, Y. Yang, J. Li, Y. Wang, J. Wang, J. Zhao, *ACS Appl. Mater. Interfaces* **2017**, *9*, 28486.
[54] C. Li, S. Dong, P. Wang, C. Wang, L. Yin, *Adv. Energy Mater.* **2019**, *9*, 1902352.
[55] Z. Li, J. Li, F. Kang, *Electrochim. Acta* **2019**, *298*, 288.
[56] Z. Li, B. Niu, J. Liu, J. Li, F. Kang, *ACS Appl. Mater. Interfaces* **2018**, *10*, 9451.
[57] J. Liu, Z. Li, X. Huo, J. Li, *J. Power Sources* **2019**, *422*, 49.
[58] S. Lu, M. Wang, F. Guo, J. Tu, A. Lv, Y. Chen, S. Jiao, *Chem. Eng. J.* **2020**, *389*, 124370.
[59] J. Tu, M. Wang, X. Xiao, H. Lei, S. Jiao, *ACS Sustainable Chem. Eng.* **2019**, *7*, 6004.
[60] S. Wang, S. Jiao, J. Wang, H.-S. Chen, D. Tian, H. Lei, D.-N. Fang, *ACS Nano* **2017**, *11*, 469.

[61] W. Xing, D. Du, T. Cai, X. Li, J. Zhou, Y. Chai, Q. Xue, Z. Yan, *J. Power Sources* **2018**, *401*, 6.
[62] Q. Yan, Y. Shen, Y. Miao, M. Wang, M. Yang, X. Zhao, *J. Alloys Compd.* **2019**, *806*, 1109.
[63] Z. Zhao, Z. Hu, R. Jiao, Z. Tang, P. Dong, Y. Li, S. Li, H. Li, *Energy Storage Mater.* **2019**, *22*, 228.
[64] N. Jayaprakash, S. K. Das, L. A. Archer, *Chem. Commun.* **2011**, *47*, 12610.
[65] N. S. Hudak, *J. Phys. Chem. C* **2014**, *118*, 5203.
[66] D.-J. Yoo, J. W. Choi, *J. Phys. Chem. Lett.* **2020**, *11*, 2384.
[67] J. Bitenc, N. Lindahl, A. Vizintin, M. E. Abdelhamid, R. Dominko, P. Johansson, *Energy Storage Mater.* **2020**, *24*, 379.
[68] M. Walter, K. V. Kravchyk, C. Böfer, R. Widmer, M. V. Kovalenko, *Adv. Mater.* **2018**, *30*, 1705644.
[69] S. Wang, S. Huang, M. Yao, Y. Zhang, Z. Niu, *Angew. Chem. Int. Ed. Engl.* **2020**, *59*, 11800.
[70] G. Studer, A. Schmidt, J. Büttner, M. Schmidt, A. Fischer, I. Krossing, B. Esser, *Energy Environ. Sci.* **2023**, *16*, 3760.
[71] M. Han, Z. Lv, L. Hou, S. Zhou, H. Cao, H. Chen, Y. Zhou, C. Meng, H. Du, M. Cai, Y. Bian, M.-C. Lin, *J. Power Sources* **2020**, *451*, 227769.
[72] Z. Liu, J. Wang, H. Ding, S. Chen, X. Yu, B. Lu, *ACS Nano* **2018**, *12*, 8456.
[73] X. Yu, B. Wang, D. Gong, Z. Xu, B. Lu, *Adv. Mater.* **2017**, *29*, 1604118.
[74] Q. Zhang, L. Wang, J. Wang, C. Xing, J. Ge, L. Fan, Z. Liu, X. Lu, M. Wu, X. Yu, H. Zhang, B. Lu, *Energy Storage Mater.* **2018**, *15*, 361.
[75] C. Zhang, R. He, J. Zhang, Y. Hu, Z. Wang, X. Jin, *ACS Appl. Mater. Interfaces* **2018**, *10*, 26510.
[76] C. Li, S. Dong, R. Tang, X. Ge, Z. Zhang, C. Wang, Y. Lu, L. Yin, *Energy Environ. Sci.* **2018**, *11*, 3201.
[77] H. Sun, W. Wang, Z. Yu, Y. Yuan, S. Wang, S. Jiao, *Chem. Commun.* **2015**, *51*, 11892.
[78] D.-Y. Wang, C.-Y. Wei, M.-C. Lin, C.-J. Pan, H.-L. Chou, H.-A. Chen, M. Gong, Y. Wu, C. Yuan, M. Angell, Y.-J. Hsieh, Y.-H. Chen, C.-Y. Wen, C.-W. Chen, B.-J. Hwang, C.-C. Chen, H. Dai, *Nat. Commun.* **2017**, *8*, 14283.
[79] M.-C. Lin, M. Gong, B. Lu, Y. Wu, D.-Y. Wang, M. Guan, M. Angell, C. Chen, J. Yang, B.-J. Hwang, H. Dai, *Nature* **2015**, *520*, 324.
[80] Z. Li, X. Wang, W. Zhang, S. Yang, *Chem. Eng. J.* **2020**, *398*, 125679.
[81] D. Wang, J. Si, S. Lin, R. Zhang, Y. Huang, J. Yang, W. Lu, X. Zhu, Y. Sun, *Inorg. Chem.* **2020**, *59*, 3239.
[82] A. Vahidmohammadi, J. Rosen, Y. Gogotsi, *Science* **2021**, *372*, eabf1581.
[83] K. R. G. Lim, M. Shekhirev, B. C. Wyatt, B. Anasori, Y. Gogotsi, Z. W. Seh, *Nat. Synth.* **2022**, *1*, 601.
[84] Z. Yuan, Q. Lin, Y. Li, W. Han, L. Wang, *Adv. Mater.* **2023**, *35*, 2211527.
[85] D. A. Kuznetsov, B. Han, Y. Yu, R. R. Rao, J. Hwang, Y. Román-Leshkov, Y. Shao-Horn, *Joule* **2018**, *2*, 225.
[86] J. Xie, Y.-C. Lu, *Nat. Commun.* **2020**, *11*, 2499.